Dalton Transactions

RSC Publishing

PAPER

View Article Online
View Journal

Cite this: DOI: 10.1039/c2dt32196c

Synthesis and characterization of mono- and dinuclear phenanthroline-extended tetramesitylporphyrin complexes as well as UV-Vis and EPR studies on their one-electron reduced species†

Corinna Matlachowski and Matthias Schwalbe*

Received 21st September 2012,
Accepted 11th December 2012

DOI: 10.1039/c2dt32196c

www.rsc.org/dalton

The syntheses of mononuclear compounds based on the fused porphyrin phenanthroline ligand (**H_2-1**) and their corresponding dinuclear porphyrin bis-bipyridine ruthenium complexes are reported. The extended π-system of the ligand is able to store electron equivalents as could be proven by the single electron reduction with KC_8 (and/or Na(Hg)) followed by subsequent UV-Vis and EPR analysis. Electron reduction could also be achieved under light illumination in a dichloromethane–triethylamine mixture. The two coordination spheres of the ligand are different so that mononuclear or (hetero)dinuclear complexes can be isolated depending on the reaction conditions. We could successfully introduce Zn, Cu and Pd into the porphyrinic unit leading to a series of mononuclear (**M-1**) compounds. Further, we could attach the bis-(4,4′-di-*tert*-butyl-2,2′-bipyridine) ruthenium fragment ($Ru(tbbpy)_2^{2+}$) to obtain dinuclear (**M-1-Ru**) metal complexes. In the case of **Zn-1** an X-ray crystal structure could be obtained confirming the selective metallation in the porphyrinic unit. All metal complexes were isolated and characterized with standard analytical tools (elemental analysis, mass spectrometry and NMR (or EPR) spectroscopy).

Introduction

Constant rising world energy consumption is met with greater use of fossil fuels, which correlates to an increase in atmospheric CO_2.[1] Utilization of sunlight offers a very attractive alternative fuel source and, thus, the field of photodriven supramolecular catalysis became more and more important in recent years.[2,3] Heterooligonuclear complexes were developed, which consist of a light harvesting unit, a linker and a reaction centre, and were able to control selectivity in organometallic catalysis (*e.g.* CO_2 or proton reduction) with the help of light.[4–7] The linker has a very crucial role as it should allow for the connection of and communication between different metal centers. Additionally, the linker should possess electron storage capacity for specific applications like proton reduction.[8–12] The photoelectron created on the photosensitizer side needs to be transferred *via* the linker to the catalytic side where the reduction of the substrate takes place. As many reduction reactions are of multi-electron nature (*e.g.* two electron processes), a linker with a partial electron storage ability to accumulate those electron equivalents is desired. Several other examples for supramolecular assemblies appeared for applications like sulfoxidation,[13,14] epoxidation,[15] alcohol oxidation,[16,17] water oxidation or anchoring to semiconductor surfaces (*e.g.* dye sensitized solar cells).[18–22]

Extended π-systems as found in the ligands tetraazatetrapyridopentacene (tatpp)[23–25] and tetrapyridophenazine (tpphz)[10,26,27] proved to be very good for electron storage of up to four electrons (for tatpp). Unfortunately, the synthesis of heterodinuclear metal complexes proved to be difficult because of solubility issues and the same phenanthroline based coordination sphere on both ends of the molecules (selectivity problems). Nevertheless, several heterodinuclear complexes with the ligand tpphz and its derivatives were synthesized and successfully tested in the photodriven proton reduction.[10,28,29] Most of the systems mentioned so far contain the chromophoric $Ru(bpy)_2^{2+}$ unit. In order to use a cheaper system, porphyrin based chromophores are very attractive.

Crossley *et al.* used the tatpp motive to connect two porphyrinic units.[30,31] For solubility reasons they used 3,5-di-*tert*-butylphenyl groups instead of phenyl groups in the *meso*-position of the porphyrinic unit. They could show that both porphyrin moieties are in electrochemical communication and

Institute of Chemistry, Humboldt-Universität zu Berlin, Brook-Taylor-St. 2, 12489 Berlin, Germany. E-mail: matthias.schwalbe@hu-berlin.de; Fax: +49-30-2093-6966; Tel: +49-30-2093-7571

†Electronic supplementary information (ESI) available: Synthesis of Cu complexes and additional spectroscopic data. CCDC 888471. For ESI and crystallographic data in CIF or other electronic format see DOI: 10.1039/c2dt32196c

that multiple reversible reduction events occur. Hence, those systems should be suitable for multi-electron reduction catalysis. However, no (photo)catalytic application was tested for these systems. In further studies, different groups showed that a porphyrin moiety could be combined with a phenanthroline moiety to allow for connection of two different metal centers.[32–34] But besides their spectroscopic characterization no catalytic application was tested. Later, Liu and coworkers used the supramolecular phenanthroline-extended tetraphenylporphyrin ligand to investigate a series of metalloporphyrin phenanthroline Pd complexes **M-Porphen-Pd**, with **M** = Ni, Zn, Mg, Cu and Co, in the Heck-reaction. The metal center in the porphyrin moiety had an influence on the catalytic performance but no influence of light illumination on the product distribution could be determined.[35] Albeit multiple spectroscopic investigations concern the reduced state of porphyrin compounds, applications in catalytic reactions are rare. Examples are restricted to systems containing a redox-active metal center like iron or cobalt in the porphyrin cavity. Those are able to drive the reduction of protons, dioxygen or CO_2 if the metal center is two- or three-fold reduced by chemical, electrochemical or photochemical means.[36–41]

An interesting question that was not answered for the porphyrin phenanthroline complexes so far is whether they are able to store electrons, which can be used in subsequent catalytic transformation. Following, we will present the preparation of the newly phenanthroline-extended tetramesitylporphyrin ligand **H_2-1** as well as its mononuclear metal complexes with Zn, Cu and Pd as the central metal atom in the porphyrin coordination sphere. The phenanthroline moiety of these complexes allows for the coordination of a second metal center like $Ru(tbbpy)_2^{2+}$ which should (a) broaden the absorption properties in the visible region and (b) decrease the reduction potential of the whole complex for thermodynamically more suitable CO_2-reduction. Hence, we present for the first time the combination of a $Ru(tbbpy)_2^{2+}$ chromophore with a **H_2-1** system to yield dinuclear complexes of the type **M-1-Ru**. The structural and spectroscopic properties of these metal compounds were analyzed in detail. Further, the single electron reduced species were isolated, characterized with EPR and UV-Vis spectroscopy, and preliminary photochemical CO_2-reduction experiments were done.

Results and discussion

Synthesis and characterization

The synthesis of the compounds **Cu-1-Ru** and **Pd-1-Ru** is outlined in Fig. 1. In the case of **Cu-1**, the precursor of **Cu-1-Ru**, a slight variation of the reaction conditions published by Karpishin and coworkers[33] was used (see ESI† for further details) and higher yields could be obtained for the photo-oxidation step by using bulb light instead of sunlight. Moreover, Karpishin's copper complex included a 2,9-dimethyl-1,10-phenanthroline moiety instead of the simple phenanthroline moiety in our system. Although this is only a marginal modification it provides less steric bulk around the phenanthroline coordination sphere and allows for complex formation of sterically crowded metal precursors in a second reaction step. We found that the reaction sequence to **M-1-Ru** is not only suitable for copper porphyrins but also for palladium porphyrins (see the Experimental section for further details). This is the first time that a palladium porphyrin system is used for the described modifications and similar overall yields are obtained compared to the copper analogue. The reaction sequence starts with the synthesis of H_2TMP (tetramesitylporphyrin) following the Lindsey method.[42] H_2TMP is then metalated with either copper or palladium. If other metal centers are used (*e.g.* Zn, Mg or Ni), the third step, the nitration in the *beta*-position, does not occur selectively. Thus, a suitable central metal ion is absolutely necessary for this reaction. Reduction of the nitro group with sodium borohydride leads to the amino derivative, which is slightly unstable against photo-oxidation, but could be handled on air for a certain time. It is not possible to purify the amino product with silica column chromatography, since silica catalyzes the photo-oxidation of the amino compound. Hence, the amino compound is subsequently oxidized with air under light illumination (bulb light – 250 W). **M**TMCO_2 (**M** = Cu or Pd) can be isolated in good yield and purity as the photoproduct after chromatographic purification. Interestingly, this oxidation proceeds about 24 times faster for the palladium complex than for the corresponding copper complex and is already completed after 2 hours. Palladium porphyrins are probably better sensitizers for singlet-oxygen, which is needed for this reaction.[43] The acid-catalyzed condensation of the dioxo compound with 1,10-phenanthroline-5,6-diamine (phendiamine) leads to the metalloporphyrin phenanthroline complex (**M-1**) in very good yields. The last step, the complexation of the phen-moiety of **M-1** with bis-(4,4′-di-*tert*-butyl-2,2′-bipyridine) ruthenium(II) dichloride, is conducted under microwave irradiation for the palladium complex to get **Pd-1-Ru** in high yield. In contrast, the corresponding copper complex is prepared applying reflux in DMF for prolonged time to give **Cu-1-Ru** in quantitative yield. Under microwave irradiation, more side reactions occur in the case of **Cu-1-Ru** which were not further investigated and just led to reduced yield. Finally, **M-1-Ru** is synthesized with an overall yield of 51% (**M** = Cu) or 47% (for **M** = Pd), respectively, based on H_2TMP.

Another synthetic strategy is necessary to obtain **M-1** compounds with **M** different to Cu or Pd, *e.g.* **M** = Zn (Fig. 2). With zinc as the metal center the nitration of the porphyrin in the *beta*-position is not selective. Because of this, Karpishin demetalated the corresponding copper complex after condensation of the dioxochlorin derivative and 2,9-dimethyl-1,10-phenanthroline-5,6-diamine.[33] However, we found that this procedure is not practicable since the demetalation of **Cu-1** with sulfuric acid/trifluoro acetic acid does not proceed quantitatively and selectively in our hands. It becomes impossible to separate the metal free porphyrin from the metalated species. Thus, we decided to demetalate the copper porphyrin in an earlier step of the reaction sequence as Liu and coworkers did.[35]

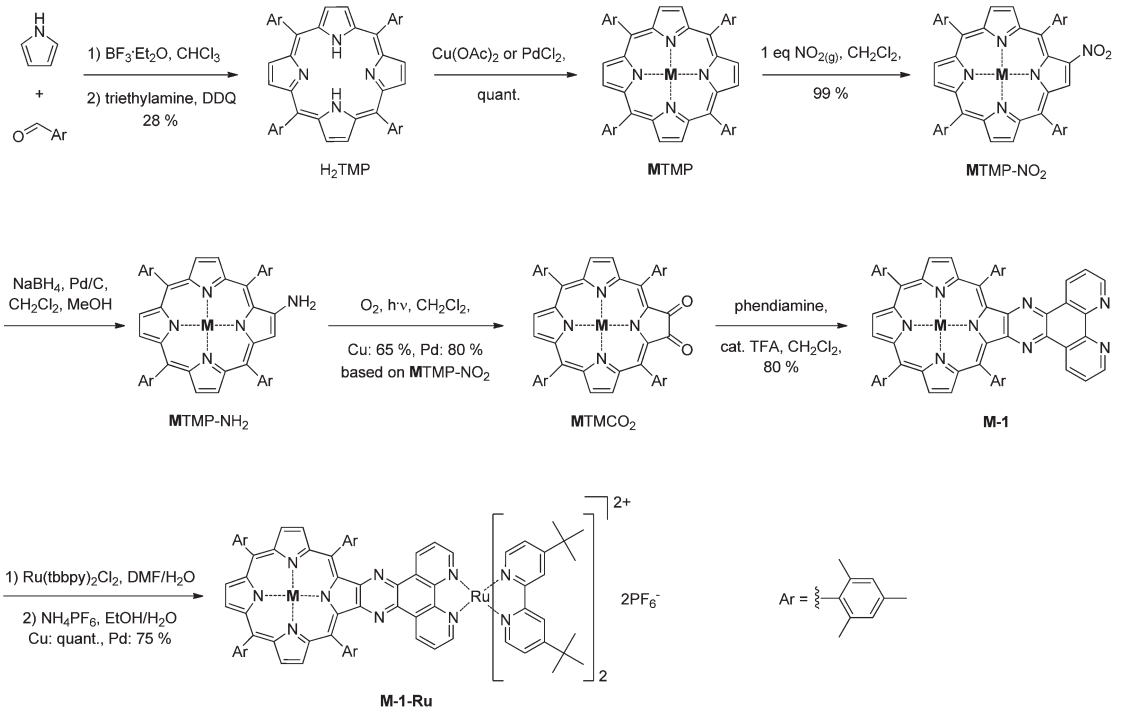

Fig. 1 Reaction sequence for the synthesis of **M-1-Ru** (**M** = Cu or Pd).

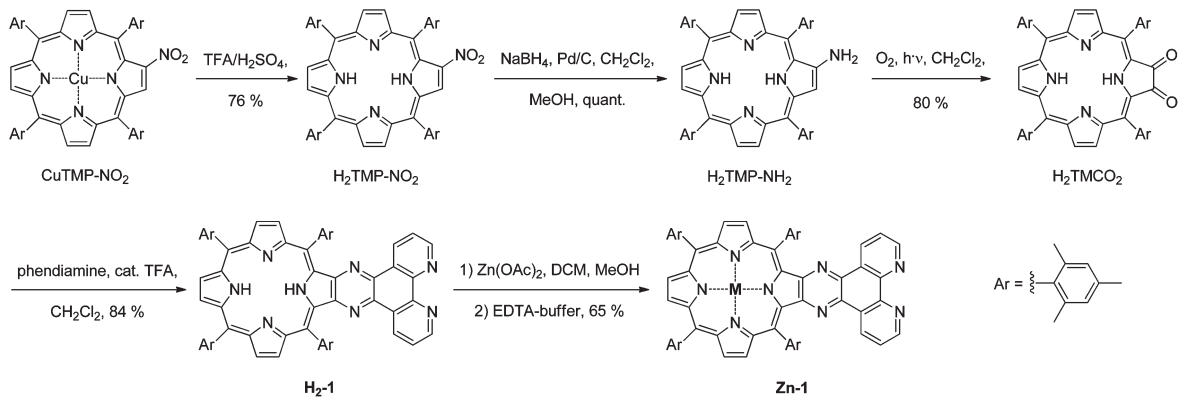

Fig. 2 Reaction sequence for the synthesis of **Zn-1**.

H_2TMP-NO_2 can easily be separated by silica column chromatography from the corresponding copper complex. The following steps to the synthesis of metal free **H_2-1** proceed smoothly and in analogy to the metalloporphyrins. **H_2-1** is obtained in an overall yield of 49% starting from CuTMP. The selective complexation of the porphyrin sphere with metal like zinc is possible while keeping the phenanthroline moiety metal free. The reaction of **H_2-1** with zinc acetate and the treatment of the reaction mixture with EDTA allows for the isolation of **Zn-1** in 65% yield. The complete synthesis of **H_2-1** and **Zn-1** is illustrated in Fig. 2.

The characterization of **H_2-1**, **Zn-1**, **Pd-1** and **Pd-1-Ru** was carried out amongst others by NMR-spectroscopy, but not for **Cu-1** or **Cu-1-Ru** due to its paramagnetism. **Cu-1** and **Cu-1-Ru** were instead characterized by EPR-spectroscopy (see EPR studies below). Further, all compounds were characterized by MALDI- or ESI-mass spectrometry (MS) as well as elemental analysis (EA). All experimental results were in agreement with the calculated ones and confirmed the molecular composition of the products. The ^{1}H-NMR-spectra in CD_2Cl_2 of **Zn-1**, **Pd-1** (Fig. 3) and **H_2-1** are quite similar. The missing NH-signal at −2.37 ppm in the spectra of **Pd-1** and **Zn-1** confirmed the presence of the metal in the porphyrin core. The chemical shifts of the pyrrolic H-atoms (H-e, H-d, H-f) seem to have no correlation to the central metal. No trend can be determined and the values are close to each other for the three considered compounds (Table 1; note that the signals H-e and H-d could not be assigned unambiguously to their respective positions in the molecule and might be interchanged). All other ^{1}H-NMR signals show basically no shift upon changing the metal

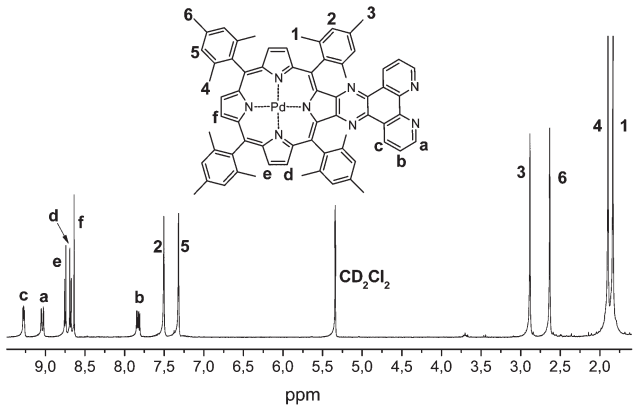

Fig. 3 The ^{1}H-NMR spectrum of **Pd-1** in CD_2Cl_2.

Table 1 ^{1}H-NMR-data of pyrrolic H-atoms of **H_2-1**, **Zn-1** and **Pd-1** in CD_2Cl_2 as well as **Pd-1-Ru** in CD_3CN (*)

	^{1}H-NMR data [ppm]		
Compound	H-e	H-d	H-f
H_2-1	8.91	8.82	8.57
Zn-1	8.85	8.79	8.68
Pd-1	8.75	8.68	8.64
Pd-1-Ru*	8.65	8.69	8.60

center in the porphyrin core. The ^{1}H-NMR-spectrum of **Pd-1-Ru** (see Fig. S1†) in CD_3CN is similar to that of **Pd-1** considering the porphyrinic signals. Besides, the *o*-methyl-groups of the mesityl-substituents are no longer equal because of the influence of the attached ruthenium fragment. The chemical shifts of the phen-protons H-a, -b and -c are influenced as well by the close proximity of the ruthenium moiety. Noteworthy is the strong shift of H-a from 9.04 ppm (for **Pd-1**) to 8.15 ppm (for **Pd-1-Ru**). H-c is also shifted to lower values (from 9.27 ppm to 8.96 ppm) in contrast to H-b whose chemical shift stays nearly the same.

Crystal structure of Zn-1

A single crystal X-ray diffraction study of **Zn-1** confirmed the formation of the desired complex with the zinc metal ion residing in the porphyrin coordination sphere and the phenanthroline-moiety staying metal free. X-ray quality crystals were obtained by covering a solution of **Zn-1** in dichloromethane (DCM) with a layer of methanol. The crystal structure of **Zn-1** (Fig. 4) includes two molecules of methanol; one is coordinated to the metal center and the non-coordinated one is incorporated into the unit cell. Selected bond lengths and angles are listed in Table 2. The zinc atom resides in an approximate square pyramidal geometry. The four nitrogen atoms of the porphyrin macrocycle form the base and one oxygen atom of a methanol molecule forms the top (Zn1–O1 = 2.080(5) Å). Interestingly, the metal–nitrogen distances to the substituted pyrrole (Zn1–N3 = 2.103(4) Å) and to the opposite one (Zn1–N1 = 2.062(4) Å) are slightly longer than to the two

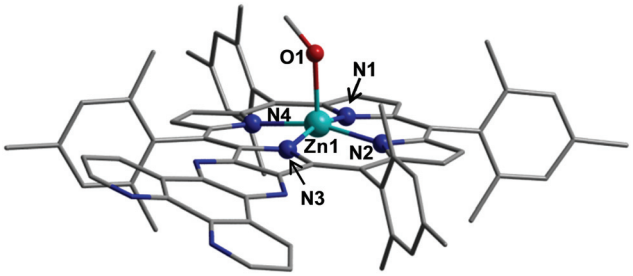

Fig. 4 The molecular structure of **Zn-1** (solvent molecules and hydrogen atoms are omitted for clarity).

Table 2 Selected bond lengths and bond angles of **Zn-1**·CH_3OH

Bond lengths [Å]		Bond angles [°]			
Zn1–N1	2.062(4)	N1–Zn1–N2	89.12(15)	N1–Zn1–O1	101.41(18)
Zn1–N2	2.033(4)	N2–Zn1–N3	88.57(15)	N3–Zn1–O1	93.35(19)
Zn1–N3	2.103(4)	N3–Zn1–N4	88.56(15)	N1–Zn1–N3	165.20(16)
Zn1–N4	2.037(4)	N4–Zn1–N1	89.59(16)	N2–Zn1–N4	163.77(16)
Zn1–O1	2.080(5)				

remaining ones (2.033(4) Å and 2.037(4) Å). This has also been observed in the crystal structures of the related species zinc tetraphenylporphyrin-phenanthroline palladium-dichloride ($ZnTPPphenPdCl_2$) from Liu[35] and iron(III) tetraphenylporphyrin quinoxaline from Wojaczyński.[44]

The zinc atom is located 0.28 Å above the plane of the four porphyrinic nitrogen atoms. Similarly, the zinc atom in Liu's complex[35] is displaced 0.32 Å out of the plane toward the axial oxygen atom of a coordinated DMSO molecule (Zn–O = 2.090 (4) Å). For **Zn-1** the dihedral angle between the phen-moiety and the modified pyrrole ring equals 14.4° which is 11° higher than in Liu's complex. This difference is due to the palladium complexation of the phen-moiety in Liu's complex. Nevertheless, the porphyrin plane of **Zn-1** is almost planar. The pyrrole rings are barely displaced alternatively above or below the mean porphyrin plane with a mean difference of 0.1 Å. Both mesityl substituents that are close to the phen-moiety are basically orthogonal to the porphyrin plane (~85°), but the angle between the other mesityl substituents and the porphyrin plane is slightly smaller (~77°).

Electrochemistry

Electrochemical investigations were done in dichloromethane solutions using tetrabutylammonium hexafluorophosphate (TBAP) as an electrolyte. Table 3 lists the redox potentials of H_2TMP, **H_2-1** and of the series of their metal complexes as well as of $[Ru(tbbpy)_2phen](PF_6)_2$. The metalated TMP compounds showed two oxidation and one reduction event. All these processes are based on the macrocycle. The **M-1** compounds showed two oxidation and two reduction events (Fig. 5). The first oxidation event is shifted to higher values in comparison to the corresponding TMP complexes due to the existence of more electron-withdrawing nitrogen atoms in the system. Interestingly, the second oxidation event does not change at all

Table 3 Redox potentials for the prepared **M**TMP, **M-1** and **M-1-Ru** compounds in DCM (*: in ACN) containing 0.1 M TBAP (EN = electronegativity)

Compound	Potential *vs.* Fc/Fc^+ [V]						
H_2TMP[46]				−1.86		0.45	
ZnTMP (EN_{Zn} = 1.6)				−2.04		0.33	0.70
CuTMP (EN_{Cu} = 1.9)				−2.00		0.45	0.88
PdTMP (EN_{Pd} = 2.2)				−1.98		0.57	1.11
H_2-1				−2.01	−1.74	0.59	
Zn-1				−2.25	−1.80	0.44	0.70
Cu-1				−2.21	−1.78	0.62	0.89
Pd-1				−2.25	−1.80	0.67	
Cu-1-Ru			−2.11	−1.91	−1.54	0.60	0.88
Cu-1-Ru*	−2.31	−2.10	−1.91	−1.81	−1.40	0.61	0.86
Pd-1-Ru			−2.09	−1.85	−1.50	0.76	0.91
$[Ru(tbbpy)_2phen](PF_6)_2$			−2.08	−1.80			0.84

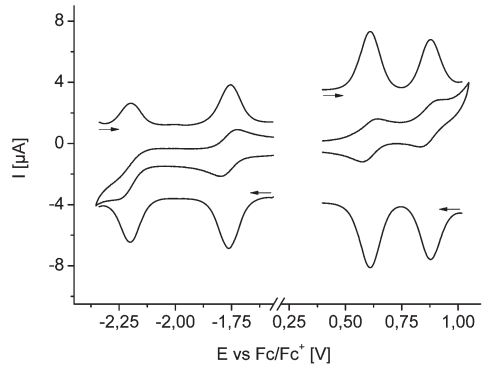

Fig. 5 Cyclovoltammogram and square-wave-voltammogram of **Cu-1** in CH_2Cl_2 containing 0.1 M TBAP.

going from **M**TMP to **M-1** for **M** = Cu and Zn. In the case of **Pd-1** a second oxidation event could not be observed probably due to restrictions of the solvent window. Surprisingly, the reduction potentials are nearly insensitive to the metal center. Similar observations could be obtained for **M-1-Ru** (**M** = Cu, Pd; Fig. S2†); however, there are two oxidation events and three reduction events occurring in the CV. In comparison to the redox potentials of $[Ru(tbbpy)_2phen](PF_6)_2$ it is clear that the Ru^{II}/Ru^{III} couple overlays with the second porphyrin oxidation (in the CV those two merge but they are slightly better resolved in the square wave voltammograms presented in Fig. S3†) and one tbbpy-centered reduction event adds to the two **H_2-1**-based reduction events. The second tbbpy-centered reduction lies probably outside of the solvent window. (If acetonitrile (ACN) is used as the solvent, five reduction events can be observed.) With regard to the **M-1** compounds, the first, very likely phenazine-centered reduction, is shifted to higher values due to ruthenium complexation. The second (and even the third) reduction of **M-1-Ru** occurs also at higher potentials than the second reduction of **M-1**.

The influence of the different metal centers on the oxidation potentials is clearly seen in a way that the more electronegative elements cause higher values of the redox potentials. Thus, the Zn complexes are the easiest to oxidize and the Pd complexes the hardest (with more than 0.2 V difference). This observation is also in line with the UV-Vis absorption properties that show the largest HOMO–LUMO gap for the Pd complexes. The second oxidation of the complex **Pd-1** could not be observed in dichloromethane. Unfortunately, it was not possible to use a different solvent for electrochemical investigations because of solubility issues with the **M-1** compounds. The dependence of the oxidation potential on the central metal was reported by Crossley and coworkers, too.[45] They investigated porphyrin quinoxaline complexes with zinc, copper, nickel or palladium as a central metal and could observe the same relation between the oxidation potential and the electronegativity of the central metal ion as we did. Thus, this fact seems to be a general property of (fused) porphyrin systems. Similar behavior could be observed for the two oxidation processes of the complexes **M-1-Ru** (**M** = Cu, Pd).

UV-Vis spectroscopy

The UV-Vis absorption spectra of the **M**TMP, **M-1** and **M-1-Ru** compounds synthesized were measured in dichloromethane and the respective maxima are summarized in Table 4. They all represent typical porphyrin spectra with a strong absorption band in the 420 nm region (Soret-band) and weaker bands in the 500–650 nm region (Q-bands). Interestingly, the different metal centers do not seem to have a great influence on the position of the Soret-band. In contrast, the position of the Q-bands depends strongly on the metal center. The Soret-band structure of **M-1** (**M** = Zn, Cu, Pd) differs significantly from that of metal-free **H_2-1** (Fig. 6 (left)). It is split into two relatively sharp peaks around 410 and 440 nm. Besides, the Soret-bands of compounds **H_2-1** and **M-1** are broadened in comparison with those of the parent **M**TMP compounds (see Fig. S4†), since the π-system of the porphyrin is extended into the phen-moiety. This also explains the bathochromic shift of the Soret band by 18 nm going from H_2TMP to **H_2-1**. The Q-band region is very sensitive to (a) the metal center and (b) the macrocycle. In the case of CuTMP and PdTMP there is only one intense band detectable at 540 nm and 526 nm while **Cu-1** and **Pd-1** show three Q-bands.

Nevertheless, in these macrocyclic series a trend in the Q-band region can be observed that shows the most hypsochromic shifts for the palladium complexes and the most bathochromic shifts for the zinc complexes. In other words,

Table 4 UV-Vis absorption maxima and emission maxima of prepared **M**TMP, **M-1** and **M-1-Ru** compounds in DCM (*: in ACN)

Compound	Absorption maxima [nm] (ε/1000 [L (mol cm)$^{-1}$])						Emission maxima [nm]
	Soret-band		Q-bands				
H_2TMP[33]	418(427)		514(18)	546(86)	590(5.5)	646(2.8)	650, 718
ZnTMP[33,47]	423(603)		547(65)	585(26)			595, 645
CuTMP	416(582)		540(24)				—
PdTMP	419(331)		526(29)				—
H_2-1	436(116)		527(7.4)	600(1.9)			655, 726
Zn-1	412(81)	446(90)	523(2.0)	570(14)	608(3.3)		615, 673
Cu-1	408(109)	444(94)	525(6.5)	563(18)	601(8.2)		—
Pd-1	403(90)	438(110)	507(4.9)	545(24)	579(12)		—
Cu-1-Ru	424(116)	472(68)	583(18)	633(sh, 4.1)			—
Cu-1-Ru*	416(128)	455(87)	573(20)	612(sh, 3.4)			—
Pd-1-Ru	416(102)	460(69)	562(22)				—

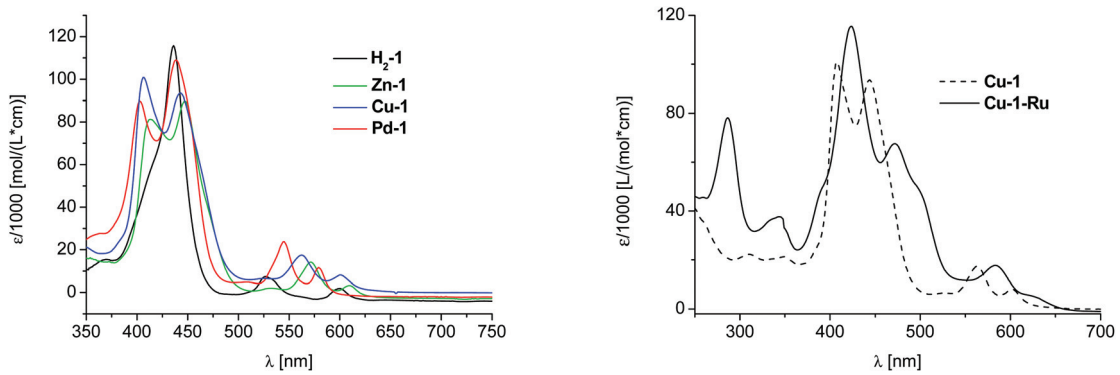

Fig. 6 UV-Vis absorption spectra in DCM of **H_2-1** and **M-1** (**M** = Zn, Cu, Pd) (left), **Cu-1** (dotted line) and **Cu-1-Ru** (solid line) (right).

the HOMO–LUMO gap increases in the order of Zn < Cu < Pd, which is reflected in the electrochemical properties too (see above).

The Soret-band of **M-1-Ru** (**M** = Cu, Pd) is shifted further bathochromic and broadened compared to the **M-1** compounds and its shape is different (see Fig. 6 (right)). The Soret-band is also split into two peaks where the peak at a lower wavelength has a higher intensity than the one at a higher wavelength. A shoulder around 500 nm appears that can tentatively be assigned to MLCT transition(s) of the ruthenium moiety. Furthermore, a band at 290 nm arises that represents π–π*-transitions of the bipyridine ligands of the ruthenium moiety.

Emission spectra can only be obtained for metal free H_2TMP and **H_2-1** as well as their zinc complexes. In the case of copper and palladium as central metals the emission is completely quenched. **H_2-1** shows emission maxima at 655 and 726 nm while **Zn-1** exhibits emission maxima at 615 and 673 nm after excitation in either the Soret- or the Q-band region. The emission maxima of **Zn-1** are blue-shifted and the intensity is smaller than for **H_2-1** if a similar concentration of the compounds is used. Karpishin and coworkers observed the same trend for **H_2-1Me$_2$** and **Zn-1Me$_2$**.[33] A similar trend is observed for the emission maxima of H_2TMP and ZnTMP too.

UV-Vis spectroscopy under reducing conditions

Stepwise reduction of **M-1** (**M** = Zn, Cu, Pd) was investigated by UV-Vis spectroscopy. To the best of our knowledge this is the first time that *chemical reduction* was performed on these kinds of complexes. **M-1** was dissolved in THF (ACN could not be used because of low solubility) and an excess of sodium amalgam (5% sodium) was added. This mixture was stirred for several hours and absorption spectra were measured every 15 minutes. The reduction reaction was slow enough to see clear changes in the UV-Vis spectra with several isosbestic points. Changes of the Soret- and Q-bands could be observed and are basically equal for all three compounds. Spectral changes are exemplarily illustrated for **Pd-1** in Fig. 7 and are discussed in the following. First, **Pd-1** is reduced to its mono-reduced species that is characterized by a diminishing Soret-band forming a new broad maximum centered at 428 nm and the appearance of three new bands at 587 nm, 622 nm and 676 nm in the Q-band region. Isosbestic points occur at 387 nm, 418 nm and 461 nm. Crossley observed similar changes in the UV-Vis spectra for the electrochemical one-electron reduction of quinoxalino-porphyrins.[48] The formation of the mono-reduced species could also be confirmed by the selective reduction of **Pd-1** with only one equivalent of Na(Hg) in THF and measuring the corresponding UV-Vis spectrum.

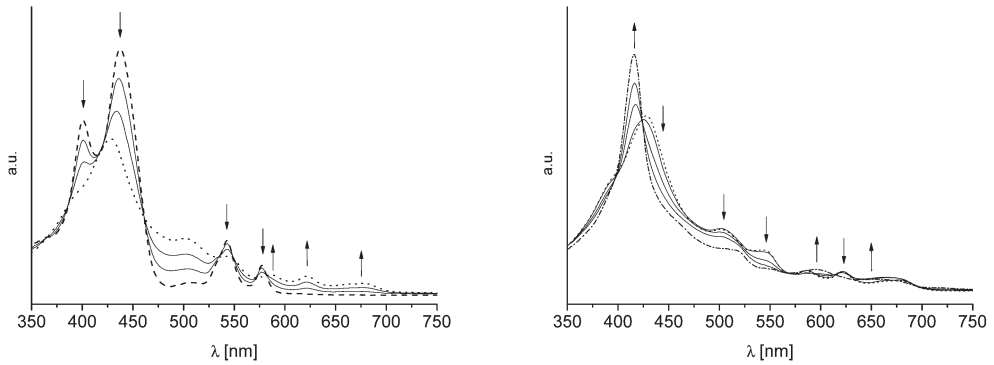

Fig. 7 Spectral changes upon mono-reduction of **Pd-1** with Na(Hg) in THF (left) and upon further reduction of the mono-reduced species to the double-reduced species (right) (dashed line: **Pd-1**, dotted line: mono-reduced species of **Pd-1 ((Pd-1)$^{-}$)**, dashed dotted line: double reduced species of **Pd-1 ((Pd-1)$^{2-}$)**, solid lines: UV-Vis spectra were measured every 15 minutes and the selected ones are shown to illustrate the progress of reaction).

The double-reduced species was formed upon further reaction with Na(Hg) and shows a thinner and blue-shifted Soret-band at 416 nm with slightly higher molar absorptivity than the mono-reduced species. Two new bands at 596 nm and 651 nm in the Q-band region are formed while the maxima corresponding to the mono-reduced species vanish. Here, isosbestic points are observed at 398 nm and 424 nm. Qualitatively similar changes in the UV-Vis spectra during the reduction with Na(Hg) could also be observed for **Zn-1** and **Cu-1** and are summarized in Table 5. Equal numbers of Q-bands are detected for the series of mono-reduced and double-reduced species.

Illumination of a THF solution of **Pd-1** containing 5% TEA with LED light (400–800 nm) shows fast changes in the UV-Vis spectrum (see Fig. S5†). Comparing the spectral appearance to the ones obtained from chemical reduction leads to the conclusion that the major species formed is the double-reduced species. However, the UV-Vis spectrum of the chemically double-reduced species does not match exactly with the spectrum after illumination. Thus, the UV-Vis spectrum after illumination is produced very likely from a mixture of multiple species including the mono- and double-reduced form as well as not identified decomposition products.

Mono-reduction of **M-1-Ru** (**M** = Cu, Pd) using Na(Hg) was also investigated by UV-Vis spectroscopy – besides spectroelectrochemistry as discussed later. Acetonitrile was chosen as a solvent, because the reduction proceeded too fast in THF to be monitored by conventional UV-Vis-spectroscopy. **M-1-Ru** was dissolved in ACN and an excess of sodium amalgam (5% sodium) was added. Changes of the Soret- and Q-bands could be observed and are basically equal for the two compounds. **Cu-1-Ru** was reduced to its mono-reduced species that is characterized by a diminishing Soret-band at 416 nm in favor of a new (split) Soret-band at 436 and 405 nm (see Fig. 8 (left) and Table 6). Clear isosbestic points are observed at 405 nm, 429 nm, 453 nm and 510 nm. Furthermore, three new bands in the Q-band region appear at 550 nm, 586 nm and 711 nm – the last one being characteristic of porphyrinic π-radical anions.[49] Similar observations could be obtained for the corresponding Pd-complex. There are two new bands in the Soret-band region at 399 nm and 436 nm. Isosbestic points are detected at 399 nm, 420 nm, 445 nm, 497 nm, 543 nm and 557 nm. In addition, three new bands in the Q-band region appear at 530 nm, 564 nm and 710 nm.

Table 5 UV-Vis absorption maxima of **M-1** (**M** = Zn, Cu, Pd) and their mono- and double-reduced species in THF

	Absorption maxima [nm]					
Compound	Soret-band(s)		Q-bands			
Zn-1	432	451	535	573	617	
(Zn-1)$^{-}$	426		576	518	643	678(br)
(Zn-1)$^{2-}$	429		428	550	615(br)	
Cu-1	409	447	526	565	603	
(Cu-1)$^{-}$	420		564	607	638	713
(Cu-1)$^{2-}$	419		520	621	706	
Pd-1	401	438	506	543	578	
(Pd-1)$^{-}$	428		505	587	622	676
(Pd-1)$^{2-}$	416		513	596	651(br)	

We believe that the first reduction event is centered on the bridging-ligand as is the case for **M-1**. Further reduction of **M-1-Ru** to the di- or triple-reduced species is complicated because of the close proximity of the second and third reduction events (see above). Thus, double or triple reduced species could not be identified unambiguously by UV-Vis spectroscopy during the reduction process – partly due to missing isosbestic points after further reduction of mono-reduced **M-1-Ru**.

UV-Vis spectroelectrochemistry

Spectroelectrochemical investigations were done in acetonitrile solutions using tetrabutylammonium hexafluorophosphate (TBAP) as an electrolyte. Measurements in dichloromethane were not possible with our setup due to the low electric conductivity of this solvent. Unfortunately, the **M-1** complexes are only marginally soluble in acetonitrile, which prevented a profound investigation. Therefore, we could only investigate

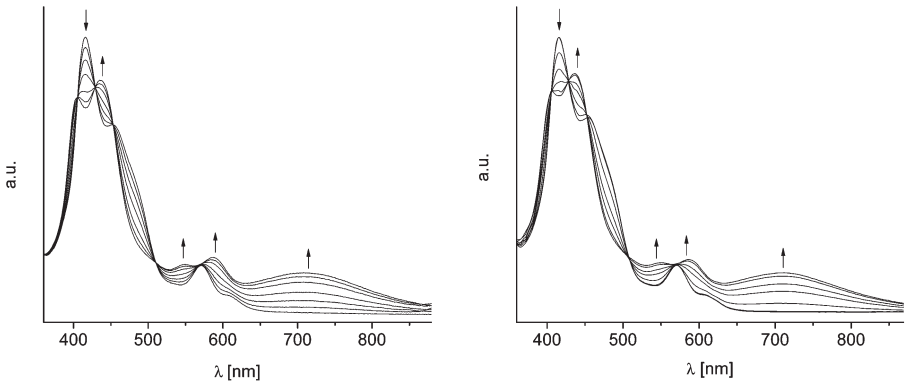

Fig. 8 Spectral changes of **Cu-1-Ru** upon either mono-reduction with Na(Hg) in ACN (left) or first *electrochemical* reduction in ACN containing 0.1 M TBAP (right).

Table 6 UV-Vis absorption maxima of **M-1-Ru** (**M** = Cu, Pd) and their mono-reduced species in ACN

	Absorption maxima [nm]				
Compound	Soret-band		Q-bands		
Cu-1-Ru	416	455	571	612(sh)	
(Cu-1-Ru)$^-$	405	436	548	588	711
Pd-1-Ru	409	446	551	584	
(Pd-1-Ru)$^-$	399	436	530	564	710

Cu-1-Ru with spectroelectrochemistry (redox potentials are listed in Table 3). Two more reduction events could be observed in ACN compared to DCM solutions, because the solvent window of ACN is larger. The first reduction at −1.40 V of **Cu-1-Ru** was examined by UV-Vis spectroelectrochemical measurements. Therefore the voltage was kept at −1.55 V and the changes in the UV-Vis spectrum during this reduction are monitored. They are essentially equal to those recorded for the sodium amalgam reduction to the mono-reduced species (see Fig. 8). The UV-Vis spectra at the end of both processes are essentially the same (see Fig. S6†) with a prominent feature at 711 nm being characteristic of a porphyrinic π-radical anion. Unfortunately, no further comment on the spectroscopic changes during the second or third reduction can be made as both overlay each other and, hence, no unambiguous assignment is possible (similar to the chemical reduction process).

Electron paramagnetic resonance studies

EPR investigations were done in THF or DCM and measured at 77 K. The recorded and simulated EPR-spectra of **Cu-1** are shown in Fig. 9. The spectrum of **Cu-1-Ru** is equal to that of **Cu-1** and clearly demonstrates an axial Cu^{II}-signal, which shows a hyperfine coupling with the four nitrogen atoms of the porphyrin unit. We also determined *g*-values and coupling constants for CuTMP, which agree well with reported values (Table 7).[50] The parameters for both compounds, **Cu-1** and CuTMP, are quite similar indicating that the phenanthroline moiety has almost no influence on the EPR-spectra, except that the parameters are barely more anisotropic ($g_x \neq g_y$, $A_x(\mathrm{Cu}) \neq A_y(\mathrm{Cu})$). The additional $Ru(tbbpy)_2^{2+}$ fragment *has no influence* on the EPR parameters.

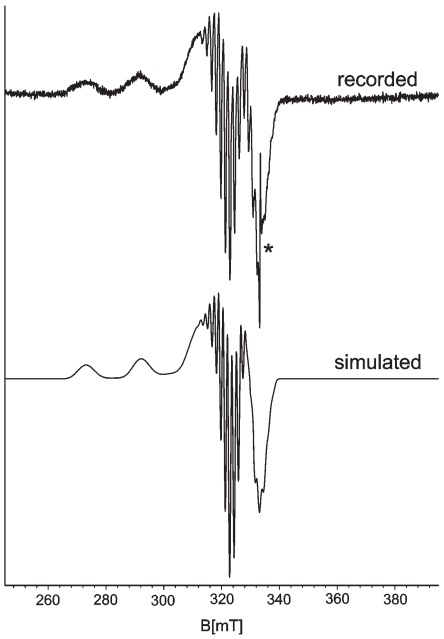

Fig. 9 Recorded and simulated EPR-spectrum of **Cu-1**/**Cu-1-Ru**. (* internal standard: $MgO:Cr^{3+}$, $g' = 1.9796$).

Ligand **1** was designed to function as an electron storage device. Thus, we investigated the possibility of storing an electron with the help of EPR-spectroscopy. One electron reduction was done either chemically using KC_8 or Na(Hg) or photochemically using triethylamine (TEA) as the sacrificial electron donor. First, we used zinc as a redox inactive central metal in the porphyrin unit. **Zn-1** was reduced by one equivalent of KC_8 (or Na(Hg)) in THF. The solution was filtered subsequently to abstract the formed graphite (or mercury) and the EPR-spectrum of this solution at 77 K showed a ligand based organic radical with $g = 2.003$ which is very close to the value of a free electron ($g = 2.0023$). The same signal could be obtained for **Pd-1**; the *g*-value is also 2.003. Surprisingly, Crossley *et al.* observed for their quinoxalino-porphyrins hyperfine coupling to the nitrogen atoms of the porphyrin sphere,[48] which we do

Table 7 EPR-parameters from simulated spectra of CuTMP and **Cu-1**/**Cu-1-Ru**

Compound	g_x	g_y	g_z	A_x(Cu)[a]	A_y(Cu)[a]	A_z(Cu)[a]	A(N)[a]
CuTMP[50]	2.031	2.031	2.185	26	26	208	16
Cu-1/**Cu-1-Ru**	2.053	2.057	2.190	17	20	190	15

[a] Hyperfine coupling constants in units of 10^{-4} cm^{-1}.

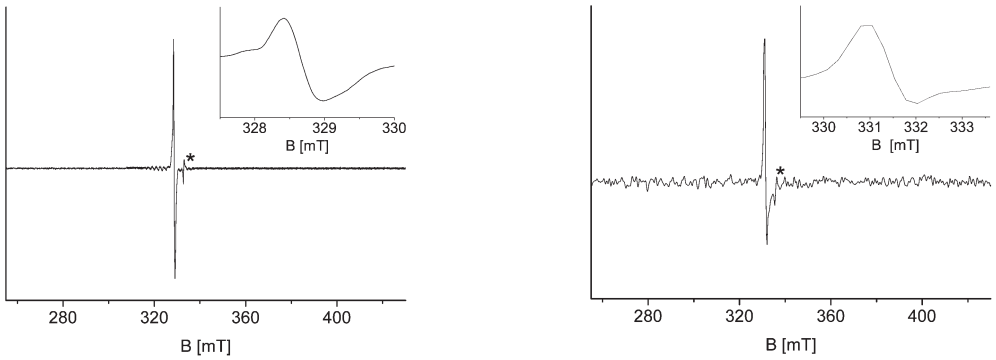

Fig. 10 Left: EPR-spectrum of photochemically mono-reduced **Pd-1**/**Pd-1-Ru**. Right: EPR-spectrum of chemically mono-reduced **Pd-1**/**Pd-1-Ru** (* internal standard: MgO : Cr^{3+}, g' = 1.9796).

not observe in the case of our phenanthroline appended porphyrins. In contrast, no organic radical based signal could be detected when **Cu-1** or **Cu-1-Ru** was reacted with one equivalent of KC_8. Instead, the copper-based signal nearly disappeared in both cases indicating an interaction of the unpaired electron of copper with a possibly formed ligand based radical. Another possibility is that Cu^{II} is reduced to Cu^{I} which is EPR-silent. But we disfavor this possibility for two reasons: (a) the very similar electrochemical behavior of **Cu-1** compared to **Zn-1** and **Pd-1** (no indication of an additional peak for the Cu^{II}/Cu^{I} couple is noticeable); thus, for **M-1** the first reduction should be centered on the ligand **1**; and (b) we do not see any formation of free **H_2-1** in the ESI-MS which would result from the loss of Cu^{I} out of the porphyrinic pocket.[51] To the best of our knowledge there is no Cu^{I} porphyrin compound presently known in the literature – very likely due to its instability.[52]

The photochemical electron transfer was investigated for **M-1** (**M** = Zn, Pd, Cu), **Pd-1-Ru** and **Cu-1-Ru**. Because of very low solubility of the **M-1** compounds in acetonitrile or THF, dichloromethane was used as a solvent. 5% TEA was added to the solution of **M-1** or **M-1-Ru** in DCM and this solution was illuminated for 5 min with LED light (*ca.* 400–800 nm) and afterwards rapidly cooled to liquid nitrogen temperature. The EPR-spectrum at 77 K showed a ligand based organic radical with g = 2.003 for **Zn-1**, **Pd-1** and **Pd-1-Ru** which is exemplarily illustrated in Fig. 10 for **Pd-1**. The EPR-signal was not quantified but the radical signal very likely does not represent all reduced species present in solution. For **Cu-1** and **Cu-1-Ru** the double integral of the Cu^{II}-signal diminished, but again no ligand based radical was detected. Note that illumination of the neat DCM–TEA solution under the same conditions produced no EPR signal.

Thus, the chemical and photochemical electron transfer on the metalloporphyrin-phenanthroline system could be confirmed and in this way also its electron storage capability.

Fujita *et al.* could show that iron and cobalt porphyrins are able to reduce CO_2 to CO.[40,41] Currently, we are investigating whether the reduced **M-1** and **M-1-Ru** species are also able to reduce CO_2 or are able to drive other organic transformations.

Preliminary CO_2 reduction experiments with **Cu-1** and **Cu-1-Ru** in a DMF (or ACN)–triethylamine solution showed no CO_2 reduction, *i.e.* no CO formation (for experimental details see ESI†). But this can be due to the fact that the metal center is not involved in the first reduction event. Besides, no changes in the UV-Vis spectrum of **Cu-1** or **Cu-1-Ru** could be observed during illumination with LED light in THF (or ACN)–triethylamine and under CO_2 atmosphere. Small changes are only observed after prolonged illumination, but no products could be isolated or characterized (*e.g.* by mass spectrometry) so far. Illumination of **Pd-1** and **Pd-1-Ru** under the same conditions caused strong changes in the UV-Vis spectrum, but also no reduction products could be identified so far and investigation of the reaction products is still in progress. In the future we will investigate whether **M-1** compounds with redox-active metal centers are photocatalysts for CO_2 reduction.

Conclusions

We have shown the successful synthesis of the tetramesitylporphyrin phenanthroline ligand **1** as well as its metal complexes with Zn, Cu and Pd. The full reaction sequence can be conducted with palladium as the central metal center obtaining higher overall yields than for the copper congener. In a

subsequent step we could attach a bis-(4,4′-di-*tert*-butyl-2,2′-bipyridine) ruthenium ($Ru(tbbpy)^{2+}$) fragment to the ligand resulting in the formation of heterodinuclear complexes of the type **M-1-Ru** with broad absorption characteristics over the visible light spectrum. The effect of the metal ion in the porphyrinic unit on the electrochemical and spectroscopic properties was investigated in detail. Both characteristics are in correlation with a HOMO–LUMO gap that is largest for Pd as a central metal and decreases to the least electronegative metal: Zn. Thus, **Pd-1** exhibits the highest first oxidation potential and shows the energetically highest absorption maxima in the Q-band region of the UV-Vis spectrum for the series of **M-1** complexes. Interestingly, the influence of the metal center is only marginal in the Soret band region of the UV-Vis spectrum. Further, **M-1-Ru** complexes exhibit anodically shifted reduction potentials in comparison to **M-1** and therefore **M-1-Ru** should be more suitable to catalyze CO_2-reduction. We could demonstrate by EPR spectroscopy that an electron can be transferred (and stored) in the delocalized ligand system by either chemical reduction with $Na(Hg)/KC_8$ or photochemical reduction with TEA/light in dichloromethane. The EPR studies were extended to UV-Vis spectroscopic characterization (either by chemical, photochemical or electrochemical reduction) of the mono-reduced **M-1-(Ru)** species. To the best of our knowledge this is the first time that chemical as well as electrochemical reduction was performed on this type of ligand showing results that are in very good agreement. Preliminary experiments to use the complexes in photocatalytic CO_2 reduction were not successful. Currently, we try to optimize the catalytic conditions and investigate the change of the metal center in the porphyrinic sphere.

Experimental section

General methods

Silica gel for column chromatography was obtained from VWR or Acros (Silica Gel 60, 230–400 μm mesh). All solvents (tetrahydrofuran (THF), toluene, dichloromethane (DCM), dimethylformamide (DMF), dimethylsulfoxide (DMSO), hexane, ethyl acetate, acetonitrile (ACN) and methanol) and most starting materials were obtained from Sigma-Aldrich. If necessary, solvents were purified employing an MBraun Solvent Purification System. Starting materials were used without further purification. Tetramesitylporphyrin (H_2TMP) was prepared using the Lindsey-method.[42] 5,6-Diamino-1,10-phenanthroline (phendiamine),[53] bis(4,4′-di-*tert*-butyl-2,2′-bipyridine) ruthenium(II) chloride ($Ru(tbbpy)_2Cl_2$),[54] bis(4,4′-di-*tert*-butyl-2,2′-bipyridine)-phenanthroline ruthenium(II) $[Ru(tbbpy)_2phen](PF_6)_2$,[54] CuTMP, CuTMP-$NO_2$, CuTMP-$NH_2$, $CuTMCO_2$, **Cu-1**[33] and PdTMP[55] were synthesized according to literature procedures with only marginal modifications as described in ESI.† PdTMP-NO_2, PdTMP-NH_2, $PdTMCO_2$, **Pd-1**,[33] H_2TMP-NO_2, H_2TMP-NH_2,[56] $TMCO_2$,[33] **H_2-1**[35] and **Zn-1**[35] were prepared following literature procedures and modified as outlined below.

^{1}H NMR spectra were recorded at ambient temperature either on a Bruker DPX-300 or on an AV-400 spectrometer. All spectra were referenced to tetramethylsilane (TMS) or deuterated chloroform ($CDCl_3$) as an internal standard (measured values for δ are given in ppm and for J in Hz). Assignment of signals was done with the help of 2D experiments. Elemental analysis was performed by the Microanalytical Lab of the Institute of Chemistry at HU Berlin using a HEKAtech EURO 3000. ESI mass spectra were obtained using Thermo Finnigan LCQ XP and LTQ FT instruments. MALDI-TOF spectra were recorded on a Bruker Daltonics REFLEX III instrument.

Absorption spectroscopic measurements were made on DCM solutions of each compound using a Cary 100 UV-vis-NIR spectrometer from Varian employing the software Cary WinUV. SUPRASIL® Quartz cells from Hellma Analytics with a 10 mm path length were used. Emission spectra were recorded on a Cary eclipse fluorescence spectrophotometer using SUPRASIL® Quartz cells from Hellma Analytics with a 10 mm path length. Emission measurements were made on DCM solutions of the investigated compounds. Cyclic voltammograms (CVs) were performed on DCM or ACN solutions containing 0.1 M NBu_4PF_6 (tetrabutylammonium hexafluorophosphate (TBAP)) and the corresponding compound under argon atmosphere at ambient temperature. A potentiostat/galvanostat PGSTAT 101 from Metrohm was used to record CVs and square wave voltammograms. A three compartment cell was outfitted with a glassy carbon button electrode as the working electrode, a platinum wire as the auxiliary electrode, and a silver wire as a pseudo-reference electrode. All data were referenced *versus* the ferrocene/ferrocenium couple at the end of each measurement. CVs were collected at scan rates of 10–100 mV s^{-1}. Square wave voltammograms were collected at an amplitude of 20 mV, a step potential of 5 mV and a frequency of 25 Hz. EPR spectra were recorded at the X-band spectrometer ERS 300 (ZWG/Magnettech Berlin/Adlershof, Germany) equipped with a fused quartz Dewar for measurements at liquid nitrogen temperature. The *g*-values were calculated with respect to a $MgO:Cr^{3+}$ reference (g' = 1.9796). The spectrum of **Cu-1** and **Cu-1-Ru** was simulated with the WINEPR simfonia package from Bruker for the calculation of powder spectra with effective *g* values and anisotropic line widths (Gaussian line shapes were used). Microwave reactions were carried out at 10–20 W in a CEM monomode microwave (model: Discover®).

{(Pyrazo[5′,6′-*e*]-1′,10′-phenanthroline)[*b*]*meso*-tetramesitylporphyrinato-copper(II)-bis(4,4′-di-*tert*-butyl-2,2′-bipyridine)-ruthenium(II)} dihexafluorophosphate (Cu-1-Ru)

Cu-1 (20 mg, 0.02 mmol) and $Ru(tbbpy)_2Cl_2$ (19 mg, 0.04 mmol, 2 equiv.) were dissolved in 30 mL DMF and 2.8 mL water. This solution was heated at 120 °C for 64 hours. The solvent was subsequently removed under reduced pressure and the product was purified by column chromatography. Impurities were first eluted with acetonitrile and the product finally with acetonitrile : water = 9 : 1 and 0.025 vol% of saturated aqueous KNO_3. After removing the solvent the product was dissolved in ethanol and aqueous ammonium hexafluorophosphate solution was added. The brown precipitate, **Cu-1-Ru**

(28 mg, 0.02 mmol, 100% based on **Cu-1**) was filtered off and washed with water and diethyl ether and dried in vacuum.

Found: C, 62.29; H, 5.06; N, 8.57. Calc. for $C_{104}H_{104}N_{12}P_2F_{12}RuCu{\cdot}1.25 \times H_2O$: C, 62.48; H, 5.37; N, 8.41; λ_{max} (DCM)/nm 286 ($\varepsilon \times 10^{-3}$/dm^3 mol^{-1} cm^{-1} 8.1), 344 (38), 424 (116), 472 (68), 583 (18), 633sh (4.1); ESI ($[M - 2PF_6^-]^{2+}$): m/z found 842.8425. Calc. for $C_{104}H_{104}N_{12}CuRu$ 842.8418; EPR-parameters (THF, 77 K, simulated): $g_x = 2.053$, $g_y = 2.057$, $g_z = 2.190$, Cu: $A_x = 17$, $A_y = 20$, $A_z = 190$, N: $A_x = A_y = A_z = 15$.

2-Nitro-*meso*-tetramesitylporphyrinatopalladium(II) (PdTMP-NO_2)

This procedure was based on a literature protocol.[33] PdTMP (100 mg, 0.11 mmol) was dissolved in 20 mL DCM in a 100 mL round-bottom flask sealed with a rubber septum. NO_2 was generated by the thermal decomposition of $Pb(NO_3)_2$ in a Schlenk-tube and was transferred in portions of 1 mL by a syringe into the reaction flask. The reaction was monitored with silica TLC (hexane : DCM = 3 : 2). When all starting material was consumed, the reaction was terminated by flushing with air to remove the remaining NO_2 gas. The solvent was removed under reduced pressure. The solid residue was suspended in hexane and loaded on a silica column packed with hexane. The dark red product, PdTMP-NO_2 (102 mg, 0.11 mmol, 99%), was eluted with a gradient of DCM and hexane (DCM: 10–37.5%; 7.5% per 200 mL).

Found: C, 73.22; H, 6.62; N, 6.58. Calc. for $C_{56}H_{51}N_5O_2Pd{\cdot}1.25 \times C_6H_{14}$: C, 73.32; H, 6.64; N, 6.73; λ_{max} (DCM)/nm 421 ($\varepsilon \times 10^{-3}$/dm^3 mol^{-1} cm^{-1} 179), 529 (17), 567 (5.9); ^{1}H NMR (300 MHz, $CDCl_3$, 25 °C): δ = 1.83 (s, 12H), 1.84 (s, 6H), 1.87 (s, 6H), 2.57 (s, 3H), 2.60 (s, 3H), 2.61 (s, 6H), 7.16 (s, 2H), 7.25 (s, 6H), 8.53 (dd, J = 5.0 and 8.1 Hz, 2H), 8.59–8.56 (m, 4H), 8.82 (s, 1H); ^{13}C NMR (75 MHz, $CDCl_3$, 25 °C): δ = 21.39, 21.43, 21.47, 21.60, 21.65, 118.77, 119.84, 120.03, 121.87, 124.69, 127.71, 127.90, 128.00, 129.47, 130.63, 130.80, 131.02, 131.12, 131.19, 131.97, 134.35, 134.81, 136.85, 137.26, 138.03, 138.36, 138.90, 139.13, 140.20, 141.15, 142.25, 142.46, 142.51, 142.62, 142.75, 149.67; MS(MALDI/TOF) (M^+): m/z found 931.6. Calc. for $C_{56}H_{51}N_5O_2Pd$ 932.5.

2-Amino-*meso*-tetramesitylporphyrinatopalladium(II) (PdTMP-NH_2)

This procedure was based upon a literature protocol.[33] PdTMP-NO_2 (133 mg, 0.14 mmol) was dissolved in 30 mL dry DCM and 10 mL dry methanol under argon atmosphere and 120 mg Pd (10% on carbon) was added. Sodium borohydride (75 mg, 1.72 mmol) was added to the solution in small portions. The reaction mixture was stirred for 1 h and all solvent was removed subsequently under reduced pressure. The solid residue was passed through a plug of celite using DCM as an eluent. Due to the instability of the product against photo-oxidation it was used immediately for the following reaction without further purification.

2,3-Dioxo-*meso*-tetramesitylchlorinatopalladium(II) (PdTMCO_2)

This procedure was based upon a literature protocol.[33] PdTMP-NH_2 was dissolved in 20 mL DCM and the solution was illuminated (bulb light – 250 W) in an open vessel for 2 h until the color of the solution turned from red to green. The solvent was removed under reduced pressure and the solid residue purified by column chromatography. The column was packed with a 3 : 1 mix of hexane : DCM and then eluted with a gradient (25–70% of DCM, 7.5% per 200 mL). PdTMCO_2 (103 mg, 0.11 mmol, 80% based on PdTMP-NO_2) was obtained as a green powder.

Found: C, 73.25; H, 5.94; N, 5.62. Calc. for $C_{56}H_{50}N_4O_2Pd$: C, 73.31; H, 6.11; N, 5.49; λ_{max} (DCM)/nm 402 ($\varepsilon \times 10^{-3}$/dm^3 mol^{-1} cm^{-1} 115), 479 (15), 609 (2.3); ^{1}H NMR (300 MHz, $CDCl_3$, 25 °C): δ = 1.81 (s, 12H), 1.85 (s, 12H), 2.54 (s, 6H), 2.56 (s, 6H), 7.17 (s, 4H), 7.20 (s, 4H), 8.04 (d, J = 4.9 Hz, 2H), 8.23 (d, J = 4.9 Hz, 2H), 8.24 (s, 2H); ^{13}C NMR (75 MHz, $CDCl_3$, 25 °C): δ = 21.2, 21.3, 21.4, 21.5, 115.5, 126.0, 127.5, 127.8, 128.0, 128.1, 128.3, 128.6, 129.0, 129.7, 131.9, 134.9, 136.5, 137.5, 137.6, 138.2, 138.5, 139.4, 141.0, 144.0, 186.6; MS(MALDI/TOF) (M^+): m/z found 916.8. Calc. for $C_{56}H_{50}N_4O_2Pd$ 916.3.

(Pyrazo[5′,6′-*e*]-1′,10′-phenanthroline)[*b*]*meso*-tetramesityl-porphyrinato-palladium(II) (Pd-1)

This procedure was based on a literature protocol.[33] PdTMCO_2 (81 mg, 0.09 mmol) and phendiamine (60 mg, 0.29 mmol) were dissolved in 165 mL dry DCM under argon atmosphere. 0.17 mL trifluoroacetic acid was added and the reaction mixture was heated at reflux overnight. The color of the solution changed from green to dark red. The reaction mixture was subsequently washed with 5% aqueous Na_2CO_3 and water and dried over Na_2SO_4. The solvent was removed under reduced pressure and the product purified with silica column chromatography. The column was packed with DCM. Unreacted PdTMCO_2 was eluted with DCM and with a mixture of 95% DCM and 5% methanol a violet band was collected to yield **Pd-1** as a dark red-brown solid (77 mg, 0.07 mmol, 80%).

Found: C, 72.85; H, 5.18; N, 9.66. Calc. for $C_{68}H_{56}N_8Pd{\cdot}0.5 \times CH_2Cl_2$: C, 72.54; H, 5.07; N, 9.88; λ_{max} (DCM)/nm 274 ($\varepsilon \times 10^{-3}$/dm^3 mol^{-1} cm^{-1} 28), 316 (21), 403 (90), 438 (109), 507 (4.9), 545 (24), 579 (12); ^{1}H NMR (300 MHz, CD_2Cl_2, 25 °C): δ = 1.84 (s, 12H), 1.90 (s, 12H), 2.63 (s, 6H), 2.88 (s, 6H), 7.32 (s, 4H), 7.51 (s, 4H), 7.83 (dd, J = 4.2 and 8.1 Hz, 2H), 8.64 (s, 2H), 8.68 (d, J = 5.1 Hz, 2H), 8.75 (d, J = 5.1 Hz, 2H), 9.04 (dd, J = 1.8 and 8.1 Hz, 2H), 9.27 (dd, J = 1.8 and 4.5 Hz, 2H); ^{13}C NMR (75 MHz, $CDCl_3$, 25 °C): δ = 21.52, 21.58, 21.70, 117.42, 121.69, 124.23, 127.91, 128.26, 128.81, 130.05, 131.00, 131.31, 135.15, 137.53, 137.55, 138.00, 138.16, 138.84, 139.10, 139.20, 140.54, 141.02, 142.67, 148.04, 151.53, 151.56; MS (MALDI/TOF) (MH^+): m/z found 1091.7. Calc. for $C_{68}H_{57}N_8Pd$ 1091.7.

{(Pyrazo[5′,6′-*e*]-1′,10′-phenanthroline)[*b*]*meso*-tetramesitylporphyrinato-palladium(II)-bis(4,4′-di-*tert*-butyl-2,2′-bipyridine)-ruthenium(II)}dihexafluorophosphate (Pd-1-Ru)

Pd-1 (20 mg, 18 μmol) and $Ru(tbbpy)_2Cl_2$ (19 mg, 22 μmol, 1.2 equiv.) were dissolved in 30 mL DMF and 2.8 mL water. This solution was heated in a microwave cavity at 105 °C for 5 hours. The solvent was subsequently removed under reduced pressure and the product was purified by column chromatography. Unreacted **Pd-1** was first eluted with acetonitrile and the product finally with acetonitrile : water = 9 : 1 and 0.025 vol% of saturated aqueous KNO_3. After removing the solvent the product was dissolved in ethanol and aqueous ammonium hexafluorophosphate solution was added. The red precipitate, **Pd-1-Ru** (28 mg, 14 μmol, 75%) was filtered off and washed with water and diethyl ether and dried in vacuum.

λ_{max} (DCM)/nm 287 ($\varepsilon \times 10^{-3}$/dm^3 mol^{-1} cm^{-1} 72), 416 (102), 460 (69), 562 (22); ^{1}H NMR (400 MHz, CD_3CN, 25 °C): δ = 1.35 (s, 18H), 1.48 (s, 18H), 1.73–1.83 (m, 24H), 2.58 (s, 6H), 2.78 (s, 6H), 7.21 (dd, J = 1.6 and 6.3 Hz, 2H), 7.32 (s, 2H), 7.33 (s, 2H), 7.43 (s, 2H), 7.50 (m, 4 H), 7.56 (d, J = 6.0 Hz, 2H), 7.74 (d, J = 6.0 Hz, 2H), 7.88 (dd, J = 5.5 and 8.3 Hz, 2H), 8.14 (d, J = 5.5 Hz, 2H), 8.51 (d, J = 1.6 Hz, 2H), 8.57 (d, J = 2.0 Hz, 2H), 8.60 (s, 2H), 8.65 (d, J = 5.2 Hz, 2H) 8.69 (d, J = 4.8 Hz, 2H), 8.96 (d, J = 8.3 Hz, 2H); ^{13}C NMR (125 MHz, CD_3CN, 25 °C): δ = 21.43, 21.45, 21.49, 21.53, 21.62, 21.65, 30.38, 30.49, 36.21, 36.35, 118.23, 118.62, 122. 42, 122.50, 122.87, 125.57, 127.75, 128.79, 129.09, 131.24, 131.98, 132.16, 132.17, 134.17, 137.98, 138.73, 138.86, 139.15, 139.43, 139.70, 140.05, 141.58, 142.11, 143.52, 149.68, 150.68, 152.10, 152.39, 153.93, 157.69, 158.07, 163.56, 163.74; ESI ($[M - 2PF_6^-]^{2+}$): m/z found 864.3295. Calc. for $C_{104}H_{104}N_{12}PdRu$ 864.3287.

2-Nitro-*meso*-tetramesitylporphyrin (H_2TMP-NO_2)

This procedure was based upon a literature method.[56] 2 mL concentrated sulfuric acid was added dropwise to a suspension of CuTMP-NO_2 (120 mg, 0.13 mmol) in 9 mL trifluoroacetic acid and stirred for 2.5 h. The suspension was poured into 150 mL water and neutralized with saturated aqueous $NaHCO_3$ and extracted three times with chloroform. The organic layers were combined, washed with water and dried over Na_2SO_4. H_2TMP-NO_2 was purified by silica column chromatography (hexane : DCM = 3 : 1) and obtained as a violet-brown solid (86 mg, 0.10 mmol, 80%). The product was characterized according to the literature.[56]

2-Amino-*meso*-tetramesitylporphyrin (H_2TMP-NH_2)

This procedure was based upon the literature method.[56] H_2TMP-NO_2 (69 mg, 0.08 mmol) was dissolved in 16 mL dry DCM and 4 mL dry methanol under argon atmosphere and Pd (10% on carbon, 75 mg) was added to the solution. Sodium borohydride (79 mg, 2.01 mmol) was added in small portions and the reaction mixture was stirred for 1 h. After removal of the solvent under vacuum the solid residue was passed through a plug of celite using DCM as an eluent. Due to the instability of the product against photo-oxidation it was used immediately for the following reaction without further purification.

2,3-Dioxo-*meso*-tetramesitylchlorin (H_2TMCO_2)

This procedure was based upon a literature protocol.[33] H_2TMP-NH_2 was dissolved in 40 mL DCM. Silica (270 mg) was added and the reaction mixture was illuminated (bulb light – 250 W) in an open vessel for 2 h. After removal of the solvent under vacuum the solid residue was purified by silica column chromatography (hexane : DCM = 3 : 2) to afford TMCO_2 (54 mg, 0.07 mmol, 80%) as a brown solid. The product was characterized according to the literature.[56]

(Pyrazo[5′,6′-*e*]-1′,10′-phenanthroline)[*b*]*meso*-tetramesitylporphyrin-phenanthroline (H_2-1)

This procedure was based on a literature protocol.[35] TMCO_2 (156 mg, 0.19 mmol) and phendiamine (140 mg, 0.65 mmol) were dissolved in 35 mL dry DCM under argon atmosphere. 0.13 mL trifluoroacetic acid was added and the reaction mixture was heated at reflux overnight. The reaction mixture was subsequently washed with 5% aqueous Na_2CO_3 and water and dried over Na_2SO_4. After removal of the solvent under vacuum the solid residue was purified with silica column chromatography. The column was packed with DCM and unreacted TMCO_2 was eluted with DCM, first. Changing to a mixture of 95% DCM and 5% methanol eluted a brown band that was collected to yield **H_2-1** as violet/brown solid (155 mg, 0.16 mmol, 84%).

Found: C, 82.23; H, 11.09; N, 5.89. Calc. for $C_{68}H_{58}N_8$: C, 82.73; H, 11.35; N, 5.92; λ_{max} (DCM)/nm 436 ($\varepsilon \times 10^{-3}$/dm^3 mol^{-1} cm^{-1} 115), 527 (7.4), 600 (1.9); ^{1}H NMR (300 MHz, CD_2Cl_2, 25 °C): δ = −2.37 (s(br), 2H), 1.86 (s, 12H), 1.92 (s, 12H), 2.65 (s, 6H), 2.90 (s, 6H), 7.34 (s, 4H), 7.52 (s, 4H), 7.83 (dd, J = 4.5 and 8.3 Hz, 2H), 8.57 (s, 2H), 8.82 (d, J = 4.8 Hz, 2H), 8.91 (d, J = 4.9 Hz, 2H), 9.06 (dd, J = 1.8 and 8.4 Hz, 2H), 9.26 (dd, J = 1.8 and 4.5 Hz, 2H); ^{13}C NMR (75 MHz, $CDCl_3$, 25 °C): δ = 21.52, 21.69, 21.74, 21.76, 115.66, 119.45, 124.26, 127.43, 127.58, 127.91, 128.21, 129.04, 133.88, 135.31, 135.34, 137.63, 137.82, 137.96, 138.00, 138.28, 138.69, 139.36, 139.65, 143.81, 151.18, 151.65, 155.50; MS(MALDI/TOF) (M^+): m/z found 987.1. Calc. for $C_{68}H_{58}N_8$ 987.2.

(Pyrazo[5′,6′-*e*]-1′,10′-phenanthroline)[*b*]*meso*-tetramesitylporphyrinato-zinc(II)-phenanthroline (Zn-1)

This procedure was based on a literature protocol.[35] **H_2-1** (50 mg, 0.05 mmol) was dissolved in 10 mL DCM. A solution of zinc acetate monohydrate (44 mg, 0.20 mmol) in 2.5 mL methanol was added and the reaction mixture was heated at reflux overnight. The solution was evaporated to dryness. The solid residue was dissolved in 10 mL DCM and washed with water. The organic layer was then stirred with 7 mL EDTA-buffer (H_4EDTA (29.2 mg), $Na(CH_3CO_2)$ (22.0 mg), acetic acid (0.21 mL) in 100 mL water) for 24 h. The separated organic layer was washed with 5% $NaHCO_3$ solution and water and dried over Na_2SO_4. Silica column chromatography (DCM :

methanol = 100 : 3) afforded **Zn-1** as a green/violet solid (35 mg, 0.03 mmol, 65%).

Found: C, 75.52; H, 5.55; N, 10.01. Calc. for $C_{68}H_{56}N_8Zn{\cdot}1.75 \times H_2O$: C, 75.42; H, 5.54; N, 10.35; λ_{max} (DCM)/nm 412 ($\varepsilon \times 10^{-3}$/dm^3 mol^{-1} cm^{-1} 81), 446 (90), 523 (2.0), 570 (14), 608 (3.3); ^{1}H NMR (300 MHz, CD_2Cl_2, 25 °C): δ = 1.85 (s, 12H), 1.90 (s, 12H), 2.65 (s, 6H), 2.90 (s, 6H), 7.33 (s, 4H), 7.51 (s, 4H), 7.83 (dd, J = 4.5 and 8.1 Hz, 2H), 8.68 (s, 2H), 8.79 (d, J = 4.8 Hz, 2H), 8.85 (d, J = 4.8 Hz, 2H), 9.11 (dd, J = 1.8 and 8.1 Hz, 2H), 9.26 (dd, J = 1.8 and 4.2 Hz, 2H); ^{13}C NMR (75 MHz, $CDCl_3$, 25 °C): δ = 21.52, 21.70, 21.81, 116.04, 120.96, 124.01, 127.76, 128.12, 128.80, 130.79, 131.00, 131.66, 134.69, 137.23, 137.60, 138.58, 138.75, 139.14, 139.18, 139.32, 139.45, 149.07, 149.27, 149.80, 151.60, 151.70; MS (MALDI/TOF) (M^+): m/z found 1050.6. Calc. for $C_{68}H_{56}N_8Zn$ 1050.6.

X-ray crystallographic details

Data were collected at 100 K on a STOE IPDS 2T. The structure was solved by direct methods (SHELXS-97)[57] and refined by full matrix least-squares procedures based on F^2 with all measured reflections (SHELXL-97).[57] All non-hydrogen atoms were refined anisotropically. All hydrogen atom positions were introduced at their idealized positions and were refined using a riding model. Crystallographic data (excluding structure factors) for **Zn-1** have been deposited at the Cambridge Crystallographic Data Centre as supplementary publication no. CCDC 888471.

Crystallographic data for **Zn-1**: $C_{68}H_{56}N_8O_2Zn{\cdot}2CH_3OH$, M = 1114.66, red crystals, orthorhombic, space group *Pna*21, a = 21.916(3) Å, b = 16.8022(17) Å, c = 15.7466(17) Å, α = 90.00°, β = 90.00°, γ = 90.00°, V = 5798.4(11) Å^3, Z = 4, T = 100(2) K, R_1 = 0.0585, wR_2 = 0.1092, GOF = 0.951.

Acknowledgements

We thank the German Science Foundation (DFGSCHW 1454/4-1) for financial support, Ramona Metzinger for help with X-ray crystallography and Prof. Stößer for his help with EPR spectra. Further, we thank Philipp Kurz and his group for help with spectroelectrochemistry.

References

1 D. G. Nocera, *Chem. Soc. Rev.*, 2009, **38**, 13–15.
2 N. Armaroli and V. Balzani, *Angew. Chem., Int. Ed.*, 2007, **46** (1–2), 52–66.
3 N. Lewis and D. G. Nocera, *Proc. Natl. Acad. Sci. U. S. A.*, 2006, **103**(43), 15729–15735.
4 S. Rau, D. Walther and J. G. Vos, *Dalton Trans.*, 2007, 915–917.
5 A. Inagaki and M. Akita, *Coord. Chem. Rev.*, 2010, **254** (11–12), 1220–1239.
6 H. Ozawa and K. Sakai, *Chem. Commun.*, 2011, **47**(8), 2227–2242.
7 M. Schulz, M. Karnahl, M. Schwalbe and J. G. Vos, *Coord. Chem. Rev.*, 2012, **256**(15–16), 1682–1705.
8 S. M. Molnar, G. Nallas, J. S. Bridgewater and K. J. Brewer, *J. Am. Chem. Soc.*, 1994, **116**(12), 5206–5210.
9 J. Hawecker, J.-M. Lehn and R. Ziessel, *New J. Chem.*, 1983, **7**, 271–277.
10 S. Rau, B. Schäfer, D. Gleich, E. Anders, M. Rudolph, M. Friedrich, H. Görls, W. Henry and J. G. Vos, *Angew. Chem., Int. Ed.*, 2006, **45**(37), 6215–6218.
11 T. A. White, B. N. Whitaker and K. J. Brewer, *J. Am. Chem. Soc.*, 2011, **133**(39), 15332–15334.
12 M. Ogawa, G. Ajayakumar, S. Masaoka, H.-B. Kraatz and K. Sakai, *Chem.–Eur. J.*, 2011, **17**(4), 1148–1162.
13 O. Hamelin, P. Guillo, F. Loiseau, M.-F. Boissonnet and S. Ménage, *Inorg. Chem.*, 2011, **50**(12), 7952–7954.
14 P. Guillo, O. Hamelin, P. Batat, G. Jonusauskas, N. D. McClenaghan and S. Ménage, *Inorg. Chem.*, 2012, **51** (4), 2222–2230.
15 C. Herrero, J. L. Hughes, A. Quaranta, N. Cox, A. W. Rutherford, W. Leibl and A. Aukauloo, *Chem. Commun.*, 2010, **46**(40), 7605–7607.
16 W. Chen, F. N. Rein, B. L. Scott and R. C. Rocha, *Chem. –Eur. J.*, 2011, **17**(20), 5595–5604.
17 W. Chen, F. N. Rein and R. C. Rocha, *Angew. Chem., Int. Ed.*, 2009, **48**(51), 9672–9675.
18 B. Gholamkhass, K. Koike, N. Negishi, H. Hori, T. Sano and K. Takeuchi, *Inorg. Chem.*, 2003, **42**(9), 2919–2932.
19 J. A. Treadway, J. A. Moss and T. J. Meyer, *Inorg. Chem.*, 1999, **38**(20), 4386–4387.
20 J. J. Concepcion, J. W. Jurss, P. G. Hoertz and T. J. Meyer, *Angew. Chem., Int. Ed.*, 2009, **48**(50), 9473–9476.
21 J. J. Concepcion, J. W. Jurss, M. K. Brennaman, P. G. Hoertz, A. Otavio, T. Patrocinio, N. Y. M. Iha, J. L. Templeton and T. J. Meyer, *Acc. Chem. Res.*, 2009, **42** (12), 1954–1965.
22 F. Li, Y. Jiang, B. Zhang, F. Huang, Y. Gao and L. Sun, *Angew. Chem., Int. Ed.*, 2012, **51**(10), 2417–2420.
23 N. R. de Tacconi, R. O. Lezna, R. Konduri, F. Ongeri, K. Rajeshwar and F. M. MacDonnell, *Chem.–Eur. J.*, 2005, **11**(15), 4327–4339.
24 R. Konduri, H. Ye, F. M. MacDonnell, S. Serroni, S. Campagna and K. Rajeshwar, *Angew. Chem., Int. Ed.*, 2002, **41**(17), 3185–3187.
25 S. Singh, N. R. de Tacconi, N. R. G. Diaz, R. O. Lezna, J. Muñoz Zuñiga, K. Abayan and F. M. MacDonnell, *Inorg. Chem.*, 2011, **50**(19), 9318–9328.
26 C. Chiorboli, M. A. J. Rodgers and F. Scandola, *J. Am. Chem. Soc.*, 2003, **125**(2), 483–491.
27 W. Paw, W. B. Connick and R. Eisenberg, *Inorg. Chem.*, 1998, **37**(16), 3919–3926.
28 S. Tschierlei, M. Karnahl, M. Presselt, B. Dietzek, J. Guthmuller, L. González, M. Schmitt, S. Rau and J. Popp, *Angew. Chem., Int. Ed.*, 2010, **49**(23), 3981–3984.
29 M. Karnahl, C. Kuhnt, F. Ma, A. Yartsev, M. Schmitt, B. Dietzek, S. Rau and J. Popp, *ChemPhysChem*, 2011, **12** (11), 2101–2109.

30 M. J. Crossley and P. L. Burn, *J. Chem. Soc., Chem. Commun.*, 1987, 39–40.
31 K. Sendt, L. A. Johnston, W. A. Hough, M. J. Crossley, N. S. Hushand and J. R. Reimers, *J. Am. Chem. Soc.*, 2002, **124**(32), 9299–9309.
32 M. J. Crossley, P. L. Burn, S. J. Langford and J. K. Prashar, *J. Chem. Soc., Chem. Commun.*, 1995, 1921–1923.
33 T. A. Vanelli and T. B. Karpishin, *Inorg. Chem.*, 2000, **39**(2), 340–347.
34 T. A. Vanelli and T. B. Karpishin, *Inorg. Chem.*, 1999, **38** (10), 2246–2247.
35 R.-S. Lin, M.-R. Li, Y.-H. Liu, S.-M. Peng and S.-T. Liu, *Inorg. Chim. Acta*, 2010, **363**(13), 3523–3529.
36 I. Bhugun, D. Lexa and J.-M. Saveant, *J. Am. Chem. Soc.*, 1996, **118**(16), 3982–3983.
37 J. A. Goodwin and T. S. Kurtikyan, *J. Porphyrins Phthalocyanines*, 2011, **15**, 99–105.
38 A. J. Olaya, D. Schaming, P.-F. Brevet, H. Nagatani, T. Zimmermann, J. Vanicek, H.-J. Xu, C. P. Gros, J.-M. Barbe and H. H. Girault, *J. Am. Chem. Soc.*, 2012, **134** (1), 498–506 and references therein.
39 J. Rosenthal and D. G. Nocera, *Acc. Chem. Res.*, 2007, **40**(7), 543–553.
40 D. Behar, T. Dhanasekaran, P. Neta, C. M. Hosten, D. Ejeh, P. Hambright and E. Fujita, *J. Phys. Chem. A*, 1998, **102**(17), 2870–2877.
41 J. Grodkowski, D. Behar, P. Neta and P. Hambright, *J. Phys. Chem. A*, 1997, **101**(3), 248–254.
42 J. S. Lindsey and R. W. Wagner, *J. Org. Chem.*, 1989, **54**(4), 828–836.
43 R. Beavington, P. A. Rees and P. L. Burn, *J. Chem. Soc., Perkin Trans. 1*, 1998, 2847–2852.
44 J. Wojaczyński, L. Latos-Grażyński and T. Głowiak, *Inorg. Chem.*, 1997, **36**(27), 6299–6306.
45 M. J. Crossley, P. J. Sintic, R. Walton and J. R. Reimers, *Org. Biomol. Chem.*, 2003, **1**, 2777–2787.
46 P. Ochsenbein, K. Ayougou, D. Mandon, J. Fischer, R. Weiss, R. N. Austin, K. Jayaraj, A. Gold, J. Terner and J. Fajer, *Angew. Chem.*, 1994, **106**(3), 355–357.
47 U. Eberhardt, W. Schwarz and H. Musso, *Liebigs Ann. Chem.*, 1987, 809–810.
48 K. M. Kadish, W. E, P. J. Sintic, Z. Ou, J. Shao, K. Ohkubo, S. Fukuzumi, L. J. Govenlock, J. A. McDonald, A. C. Try, Z.-L. Cai, J. R. Reimers and M. J. Crossley, *J. Phys. Chem. B*, 2007, **111**(30), 8762–8774.
49 E. Wenbo, K. M. Kadish, P. J. Sintic, T. Khoury, L. J. Govenlock, Z. Ou, J. Shao, K. Ohkubo, J. R. Reimers, S. Fukuzumi and M. J. Crossley, *J. Phys. Chem. A*, 2008, **112**, 556–570.
50 K. L. Cunningham, K. M. McNett, R. A. Pierce, K. A. Davis, H. H. Harris, D. M. Falck and D. R. McMillin, *Inorg. Chem.*, 1997, **112**(11), 608–613.
51 M. Kumar, P. Neta, T. P. G. Sutter and P. Hambright, *J. Phys. Chem.*, 1992, **96**, 9571–9575.
52 We also tried to synthesize a Cu^{I}-porphyrin, but did not succeed: reaction of $[Cu(ACN)_4](PF_6)$ with TMP results in no complex formation.
53 S. Bodige and F. M. MacDonnell, *Tetrahedron Lett.*, 1997, **38** (47), 8159–8160.
54 S. Rau, B. Schäfer, A. Grüßing, S. Schebesta, K. Lamm, J. Vieth, H. Görls, D. Walther, M. Rudolph, U. W. Grummt and E. Birkner, *Inorg. Chim. Acta*, 2004, **357**, 4496–4503.
55 M. J. Crossley, C. S. Sheehan, T. Khoury, J. R. Reimers and P. J. Sintic, *New J. Chem.*, 2008, **32**, 340–352.
56 S. Eu, S. Hayashi, T. Umeyama, Y. Matano, Y. Araki and H. Imahori, *J. Phys. Chem. C*, 2008, **112**(11), 4396–4405.
57 G. M. Sheldrick, *Acta Crystallogr., Sect. A: Fundam. Crystallogr.*, 2008, **64**, 112–122.

